journal of the mechanical behavior of biomedical materials 155 (2024) 106557

Contents lists available at ScienceDirect

Journal of the Mechanical Behavior of Biomedical Materials

journal homepage: www.elsevier.com/locate/jmbbm

How do different intraoral scanners and milling machines affect the fit and fatigue behavior of lithium disilicate and resin composite endocrowns?

Rafaela Oliveira Pilecco [a], Lucas Saldanha da Rosa [a], Andrea Baldi [b], Renan Vaz Machry [a], João Paulo Mendes Tribst [c,*], Luiz Felipe Valandro [a], Cornelis Johannes Kleverlaan [d], Nicola Scotti [b], Gabriel Kalil Rocha Pereira [a]

[a] Post-Graduate Program in Oral Sciences (Prosthodontics Units), Faculty of Dentistry, Universidade Federal de Santa Maria (UFSM), Santa Maria, Rio Grande do Sul State, Brazil
[b] Department of Surgical Sciences, Dental School, University of Turin (UNITO), Turin, Piedmont, Italy
[c] Department of Reconstructive Oral Care, Academic Centre for Dentistry Amsterdam (ACTA), Universiteit van Amsterdam and Vrije Universiteit, Amsterdam, North Holland, the Netherlands
[d] Department of Dental Materials Science, Academic Centre for Dentistry Amsterdam (ACTA), Universiteit van Amsterdam and Vrije Universiteit, Amsterdam, North Holland, the Netherlands

ARTICLE INFO

Keywords:
CAD/CAM
Dental ceramics
Fatigue
Intraoral scanners
Marginal/internal fit
Milling machine

ABSTRACT

The aim of this in vitro study was to evaluate the effect of the combinations of two different intraoral scanners (IOS), two milling machines, and two restorative materials on the marginal/internal fit and fatigue behavior of endocrowns produced by CAD-CAM. Eight groups (n= 10) were considered through the combination of TRIOS 3 (TR) or Primescan (PS) IOS; 4-axes (CR; CEREC MC XL) or 5-axes (PM; PrograMill PM7) milling machines; and lithium disilicate (LD; IPS e.max CAD) or resin composite (RC; Tetric CAD) restorative materials. Specific surface treatments were applied to each material, and the bonding to its corresponding Endocrown-shaped fiberglass-reinforced epoxy resin preparations was performed (Variolink Esthetic DC). Computed microtomography (μCT) was performed to assess the marginal/internal fit, as well as a mechanical fatigue test (20 Hz, initial load = 100 N/5000 cycles; step-size = 50 N/10,000 cycles until a threshold of 1500 N, then, the step-size was increased if needed to 100 N/10,000 cycles until failure or a threshold of 2800 N) to evaluate the restorations long-term behavior. Complementary analysis of the fracture features and surface topography in scanning electron microscopy was performed. Three-way ANOVA and Kaplan-Meier test (α = 0.05) were performed for marginal/internal fit, and fatigue behavior data, respectively. PS scanner, CR milling machine, and RC endocrowns resulted in a better marginal fit compared to their counterparts. Still, the PM machine resulted in a better pulpal space fit compared to the CR milling machine. Regardless of the scanner and milling machine, RC endocrowns exhibited superior fatigue behavior than LD ones. LD endocrowns presented margin chipping regardless of the milling machine used. Despite minor differences in terms of fit, the 'IOS' and 'milling machine' factors did not impair the fatigue behavior of endocrowns. Resin-composite restorations resulted in a higher survival rate compared to glass-ceramic ones, independently of the digital devices used in the workflow.

1. Introduction

Diverse rehabilitation options are suggested for endodontically treated teeth, which can be performed directly or indirectly, as inlays, onlays, overlays, crowns, or endocrowns (Lenz et al., 2023; Mannocci et al., 2022). The latter involves a restoration with an extension inside the pulp chamber (usually 3–4 mm depth), indicated especially in cases with limited inter-occlusal space, as it preserves more residual tooth structure and does require less preparation height compared to conventional post-retained crowns (4–5 mm minimum of supracrestal dental tissue) (Govare and Contrepois, 2020; Mannocci et al., 2022; Saratti et al., 2021). Computer-aided-design-computer-aided-manufacturing (CAD-CAM)

* Corresponding author.
E-mail addresses: rafaela.pilecco@acad.ufsm.br (R.O. Pilecco), lucas.saldanha@acad.ufsm.br (L.S. da Rosa), andrea.baldi@unito.it (A. Baldi), renanmachry@gmail.com (R.V. Machry), j.p.mendes.tribst@acta.nl (J.P.M. Tribst), lfvalandro@gmail.com (L.F. Valandro), c.kleverlaan@acta.nl (C.J. Kleverlaan), nicola.scotti@unito.it (N. Scotti), gabriel.pereira@ufsm.br (G.K.R. Pereira).

https://doi.org/10.1016/j.jmbbm.2024.106557
Received 27 February 2024; Received in revised form 3 April 2024; Accepted 17 April 2024
Available online 18 April 2024
1751-6161/© 2024 The Author(s). Published by Elsevier Ltd. This is an open access article under the CC BY license (http://creativecommons.org/licenses/by/4.0/).

technology is one of the possible methods for fabricating endocrowns with high precision, and reduced clinical time (He et al., 2021) which evolves a sequence of steps.

The several stages in the CAD-CAM digital workflow, spanning from tooth preparation to the definitive restoration bonding, can exert an influence on the mechanical behavior of milled endocrowns. Initially, a scanning device is used to create a 3D image of the prepared teeth (Alghazzawi, 2016). This stage is executed utilizing intraoral scanners (IOS), and these devices can vary in scanning principles (i.e. active triangulation, confocal microscopy, active wavefront sampling, or even a combination of these principles) leading to potential accuracy variations (Abduljawad and Rayyan, 2022; Alghazzawi, 2016; Gurpinar and Tak, 2022; Pilecco et al., 2023). Afterward, the endocrown design is created in software, guiding the restoration's production in a milling machine using a subtractive process. Various factors introduced in this machining step, such as the number of axes, rotation speed, lubricant liquid, and the diamond burs' characteristics, can also affect the obtained restoration (Alajaji et al., 2017; Alghazzawi, 2016; Ayres et al., 2023; Blatz and Conejo, 2019; Pilecco et al., 2024).

Along with that, to fabricate via CAD-CAM the endocrowns restorations, different restorative materials have been suggested including polycrystalline ceramics, glass-ceramics, and resin composite materials (Dartora et al., 2019; Govare and Contrepois, 2020; Zheng et al., 2022a). Intrinsic material properties are directly related to the endocrown performance. Regarding elastic modulus, the higher this material property, the greater the stress concentrates within the restoration, leading to less tensile stress in the cement layer, favoring ceramic-based materials, such as lithium disilicate (He et al., 2021; Tribst et al., 2018; Yildirim et al., 2022; Zheng et al., 2022a). This material stands out due to its ability to strongly bond to the resin cement and, consequently to the tooth structure, especially considering the dependency of the bonding procedure for endocrowns due to its limited preparation height (Al-Dabbagh, 2021; Govare and Contrepois, 2020). On the contrary, a material with a lower elastic modulus, like resin-based materials, can promote a more uniform load distribution (Al-Dabbagh, 2021; Sedrez-Porto et al., 2020; Vijayakumar et al., 2021). Additionally, CAD-CAM resin composite blocks offer advantages in terms of ease of adjustment, milling, and repair (Duan and Griggs, 2015).

All those previously raised fabrication variables evolved in the CAD-CAM workflow need to be critically assessed regarding the consequences in the endocrown final aspect. One significant outcome to consider is the marginal and internal fit within the tooth structure (Hassouneh et al., 2023). Since IOS relies on the object's light transmission, the intracoronary preparation may be a challenge to the image acquisition process (Gurpinar and Tak, 2022). This may lead to poorly adapted restorations, resulting in an unfavorable biological outcome, in terms of periodontal health and facilitation of the dissolution of the bonding agent (Holmes et al., 1989; May et al., 2012). Furthermore, a thicker resin cement layer can affect the load distribution and adversely affect the fatigue behavior (Martini et al., 2019; May et al., 2012; Seo et al., 2009). It is important to consider that the intaglio surface of indirect restorations, along with the cement layer, serves as points of origin for fractures due to the concentration of tensile stress in these regions (Tribst et al., 2018; Da Fonseca et al., 2018). This susceptibility to failure, arising from fatigue, highlights the importance of meticulous attention to these areas during restoration procedures (Kruzic et al., 2018; Zhang et al., 2013).

While previous studies have individually investigated the influence of different IOS, fabrication methods, and restorative materials on the marginal and internal fit of endocrowns (Abduljawad and Rayyan, 2022; Ayres et al., 2023; Gurpinar and Tak, 2022; Hassouneh et al., 2023; Soliman et al., 2022; Zheng et al., 2022b; Zimmermann et al., 2019), more research is needed to better understand the role and consequences of each factor on the endocrowns marginal/internal fit. This knowledge is critical for comprehending their behavior under cyclic load application, a condition that restorations naturally face in the oral environment, especially considering that the clinical longevity of dental restorations will inevitably be dependent on their fatigue behavior (Kruzic et al., 2018).

Therefore, the aim of this in vitro study is to evaluate the effect of combinations between two intraoral scanners, two milling machines, and two restorative materials on both the marginal/internal fit and fatigue behavior of CAD-CAM milled endocrowns. The tested hypotheses are that different scanners (i), and milling devices (ii) would affect the marginal/internal fit of the endocrowns; that different digital workflows (iii) would result in different endocrown fatigue behavior; and that different restorative materials (iv) would respond differently for all explored outcomes.

2. Materials and methods

2.1. Study design

This in vitro study takes into consideration three factors: (i) IOS system – a confocal microscopy-based (TRIOS 3, 3Shape – TR) or with combined technology (confocal microscopy + active triangulation; CEREC Primescan AC, Dentsply Sirona – PS); (ii) milling machine – 4-axes (CEREC MC XL, Dentsply Sirona) or 5-axes (PrograMill PM7, Ivoclar AG); and (iii) CAD-CAM restorative material – lithium disilicate glass-ceramic (LD, IPS e.max CAD, Ivoclar AG) or resin composite (RC, Tetric CAD, Ivoclar AG), as illustrated in Fig. 1.

2.2. Specimen preparation

First, dies were milled using a lathe (Diplomat 3001; Nardini) on the fiberglass-reinforced epoxy resin (Protec Produtos Técnicos Ltda.) (Dalla-Nora et al., 2024; Kelly et al., 2010) considering preparation for the crown (n= 10) with a ferrule shoulder preparation (depth = 1.2 mm and radii = 0.5 mm) (Venturini et al., 2018). After, a single trained operator adapted each substrate preparation into an endocrown format (Fig. 2). A decrease in the preparation height was performed by grinding the substrate in a polishing machine (Ecomet/Automet 250, Buehler) using a diamond disk (Dia-Grid Diamond Discs #120, Allied High Tech Products, Inc.) until a preparation height of 2 mm (Dartora et al., 2018). Then, a diamond bur (FG #3131, KG Sorensen) was used in a multiplier contra-angle (Smax M95 up to 200,000 min^{-1}, Nakanishi Inc.) coupled to a micromotor (Kavo Dental). The contra-angle was fixed in a modified optical microscope (Missau et al., 2018) to ensure precision by maintaining the diamond bur perpendicular to the occlusal face of the die. A preparation simulating the pulpal chamber area (Fages and Bennasar, 2013) was carried out by deepening the diamond bur to the substrate base, in the center of the occlusal face, until its entire extension (4 mm; Fig. 2). The extrusion of each wall was defined by the inclination of the diamond bur active part, keeping an axial remainder with 2 mm of thickness.

To allow the digitalization procedure, a typodont model was adapted to allow the fitting of the different dies (Fig. 1). Each die was positioned into the model and scanned according to the study design using TR or PS. The resulting STL files were sent to each design software (TRIOS Design Studio 21.2.3, 3Shape; and CEREC 4.5.2 software, Dentsply Sirona) in which endocrowns (n= 10) with an occlusal thickness of 1.5 mm and a cement space of 120 μm were planned. Milling was performed in 4-axis (CR) or 5-axis (PM) machines. Each machine was configured properly according to the manufacturer instructions - wet-milling, step bur 12S, and cylinder pointed bur 12S for CR; PrograMill tool red g2.8, g2.0, and g1.0 for PM, considering the two restorative materials (LD or RC). Following, LD endocrowns were crystallized in a furnace according to the manufacturer's instructions (Speed Crystallization in the Programat CS4, Ivoclar AG), and RC ones remained untouched. Each endocrown was tested into its corresponding die before bonding procedures, to guarantee optimal setting.

Fig. 1. Flow chart of the study design and illustration of the adapted typodont model for the endocrown scanning procedure (TR, TRIOS 3; PS, Primescan; CR, CEREC MC XL; PM, PrograMill PM7; LD, lithium disilicate; RC, resin composite; n = 10).

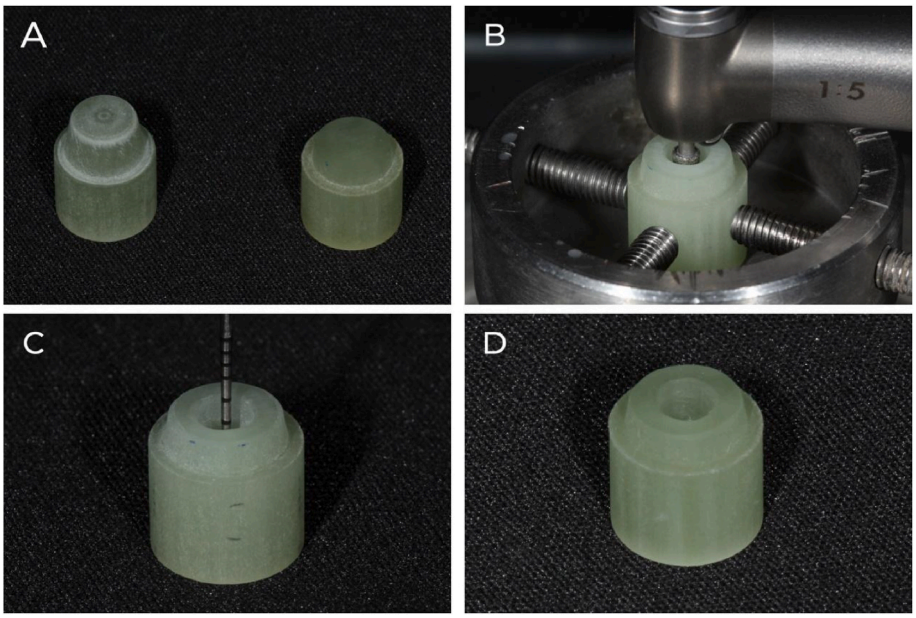

Fig. 2. Illustration of the steps to prepare the fiberglass-reinforced epoxy resin substrate to receive an endocrown restoration.

2.3. Bonding procedure

The restorations and dies were cleaned in an ultrasonic bath with 70% alcohol for 5 min. Then, each material was treated as recommended by its manufacturer or referenced in the literature. The dies were etched with hydrofluoric acid (<5% IPS Ceramic etching-gel, Ivoclar AG) for 60 s (Schestatsky et al., 2019), washed out with air-water spray for 30 s, air-dried, and received the application of a light-curing single-component dental adhesive for 20 s with posterior air-drying (Adhese Universal, Ivoclar AG), which was not light-cured. LD bonding surface was etched with <5% hydrofluoric acid for 20 s, washed out with an air-water spray for 30 s, air-dried, and a silane coupling agent was actively applied (Porcelain Silane, B.J.M. Laboratories Ltd) for 15 s, kept it to react for another 45 s and gently air-dried. RC bonding surface was sandblasted with 50 μm aluminum oxide (10 mm distance, 1 bar pressure; Ossido di Alluminio, Henry Schein),

cleaned in an ultrasonic bath with 70% alcohol for 5 min, and an adhesive was actively applied (Adhese Universal, Ivoclar AG) for 20 s with posterior air-drying, without light-curing. Finally, a dual-cure resin cement (Variolink Esthetic DC, Ivoclar AG) was manipulated, the endocrowns settled into the dies with a standardized load device (500 g), the cement excess was removed with a micro brush, and light cured (Starlight Uno, Mectron) for 40 s in each direction (0°, 90°, 180°, 270°, and on the top).

2.4. Marginal and internal fit

A computed microtomography analysis (μCT - SkyScan 1172 Micro-CT, Bruker) was run in each individual bonded specimen, with the following parameters: 100 Kv, 100 μA, source-object distance= 89.510 mm, source-detector distance= 217.578 mm, pixel binning= 9.01 μm, exposure time/projection= 846 ms, aluminum and copper (Al + Cu) filter; pixel size= 14.83 μm, averaging= 5, rotation step= 0.6°, resulting in a total of 414 slices per specimen. To reconstruct the images in a specific software (NRecon, Bruker, Billerica), different parameters were used for each restorative material (LD/RC respectively), as follows: smoothening= 0/2, misalignment compensation= 5/4.5, ring artifacts reduction= 10/2, beam-hardening correction= 30/40%. Later, for assessment of marginal and internal fit, the reconstructed images were inserted into a software (Data Viewer, Bruker Kartuizersweg 3B) to create sagittal and coronal sequential images, where three slices of each direction were selected and analyzed at ImageJ 1.53t (National Institutes of Health) (Freitas et al., 2020; Vág et al., 2020) considering 2 regions of interest (ROI) for marginal gap (Holmes et al., 1989) and 9 ROIs for internal fit (Zheng et al., 2022b), resulting in 66 measurements per specimen (Fig. 3) (Nawafleh et al., 2013). For this, a single trained operator began with the identification of the exact midpoint of the specimen. Subsequent slices were then selected in a consistent manner, utilizing directional movements (mesial and distal directions) relative to the initial slice. This systematic approach ensures a standardized process for selecting the three slices, thereby maintaining consistency and reliability in scientific measurements.

2.5. Fatigue test and fractographic analysis

A mechanical fatigue test was carried out in an electric mechanical testing machine (Instron ElectroPuls E3000, Instron) using an accelerated cyclic fatigue approach (Valandro et al., 2023) under a 20 Hz frequency (Velho et al., 2020). A stainless-steel hemispherical piston (Ø= 40 mm) was positioned in the center of the occlusal surface of the specimen immersed in distilled water. An adhesive tape (110 μm) was interposed between the piston and specimen. A 100 N load was applied first for 5000 cycles to guarantee the relation between the specimen and the piston. After that, the load was increased by 50 N for every 10,000 cycles, and the test was carried out until failure was detected or a threshold of 1500 N was reached; in case of survival up to this step (1500 N), the step was increased to 100 N for every 10,000 cycles, until failure or test completion at 2800 N. Failure detection was carried out by the specimen transillumination at the end of each step to verify the presence of cracks or fractures. Data on fatigue failure load (FFL) and number of cycles for failure (CFF) were collected for statistical analysis.

Failed specimens were analyzed qualitatively in a stereomicroscope (10 ×) and in a Scanning Electron Microscopy (SEM; VEGA-3G; Tescan) by a single trained and experienced operator (R.V.M.) to characterize the failure origin. A topographic analysis in SEM was performed in one additional specimen per group, considering the milling machines and restorative material, after it was sputter-coated with gold.

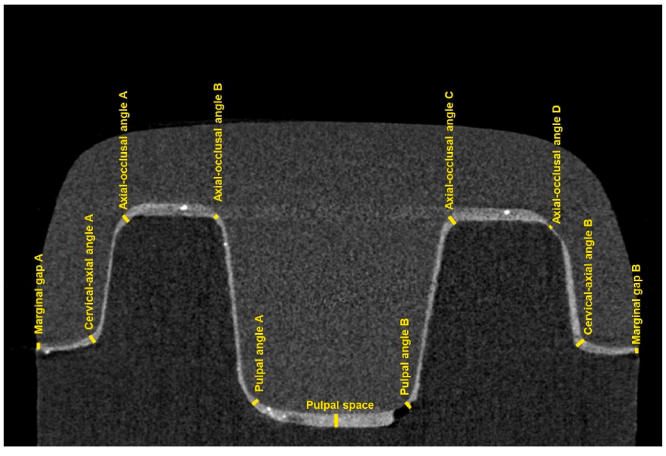

Fig. 3. Representative figure of the measured regions of interest (ROI) for the marginal and internal measurements of specimens after the μCT analysis.

2.6. Statistical analysis

A power estimation of the statistical analysis was performed (G*Power software) using a one-way Analysis of Variance (ANOVA) post hoc power analysis based on α= 0.05, sample size= 80, and effect size= 3.28 using the FFL means and the mean standard deviation. Two statistical software (IBM SPSS Software v.21, IBM; and Statistix 10, Analytical Software) were used for analyzing the different tested outcomes (α= 0.05). A three-way ANOVA was conducted for marginal/internal fit. The Kaplan-Meier test and Log-rank (Mantel-Cox) were performed for survival analysis. Furthermore, the mechanical reliability of the respective digital flows and different materials of the restorations was analyzed by Weibull Analysis (SuperSMITH Weibull 4.0k-32 software program) using the maximum likelihood estimation method (confidence interval 95%).

3. Results

The power was estimated in 1-β= 1.00 (100%). According to a three-way ANOVA, the three factors (intraoral scanner, milling machine, and restorative material), along with their interactions, exert varying effects on each outcome examined in this study (Table 1). In regard to the marginal gap (Table 1, Table 2, and Table 3), it is seen that the PS scanner, CR milling machine, and RC endocrowns exhibited superior fit in comparison to their counterparts. At the cervical-axial angle, the PS scanner and CR milling machine led to a better fit. Nevertheless, there were no significant differences when it came to different materials used. As for the axio-occlusal angle, the TR scanner resulted in a better fit, while the milling machine and the restorative material did not show significant effects. Conversely, for the pulpal angle, the IOS used was not relevant, while the PM machine and LD restorations exhibited a better fit. There was no difference between the IOS and the restorative materials in the pulpal space, but the use of the PM machine resulted in a better fit.

Considering the fatigue behavior outcomes (Table 1, Table 4, and Fig. 4), the combination of TR scanner and PM milling machine yielded worse fatigue behavior compared to TR-CR and PS-PM ($P< 0.05$). Nevertheless, irrespective of the scanner and milling machine used, resin-based endocrowns exhibited higher FFL and CFF than LD ones ($P< 0.05$). The combination of PS and PM devices resulted in higher survival rate for LD compared to PS-CR and TR-CR ($P< 0.05$), although it was similar to TR-PM ($P> 0.05$). The mechanical reliability was not different among the tested groups (Table 4).

Fractographic analysis showed that failures initiated from the restoration inner surface and grew towards the occlusal surface of the endocrowns (Fig. 5). It is possible to visualize multiple directions of crack propagations, arrest lines, and the compression curl, indicating that the failure occurred and propagated during the fatigue test/cyclic load application. In this sense, the main critical area to initiate the fracture seems to be concentrated in the internal axio-occlusal angles. A

Table 1
Three-way ANOVA for marginal, internal fit, and fatigue failure load data, considering the factors intraoral scanner, milling machine, restorative material, and their association.

Marginal gap						Cervical-Axial angle					
Factors	SS	DF	MS	F	*P*	Factors	SS	DF	MS	F	*P*
Scanner device	42,947	1	42,947	5.95	**0.015**	Scanner device	21,613	1	21,613	5.11	**0.024**
Milling machine	40,547	1	40,547	5.62	**0.018**	Milling machine	62,905	1	62,905	14.86	**0.001**
Material	31,591	1	31,591	4.38	**0.037**	Material	9888	1	9888	2.34	0.127
Scanner[a]Milling machine	161,746	1	161,746	22.42	**<0.001**	Scanner[a]Milling machine	12,812	1	12,812	3.03	0.082
Scanner[a]Material	33,217	1	33,217	4.60	**0.032**	Scanner[a]Material	17,468	1	17,468	4.13	**0.042**
Milling machine[a]Material	54,647	1	54,647	7.58	**0.006**	Milling machine[a]Material	43,484	1	43,484	10.28	**0.001**
Scanner[a]Milling machine[a]Material	2092	1	2092	0.29	0.590	Scanner[a]Milling machine[a]Material	7532	1	7532	1.78	0.182
Axial-occlusal angle						*Pulpal Angle*					
Factors	SS	DF	MS	F	*P*	Factors	SS	DF	MS	F	*P*
Scanner device	50,584	1	50,584	12.09	**0.001**	Scanner device	10,441	1	10,441	0.90	0.342
Milling machine	6153	1	6153	1.47	0.225	Milling machine	408,045	1	408,045	35.27	**<0.001**
Material	2928	1	2928	0.70	0.403	Material	292,392	1	292,392	25.27	**<0.001**
Scanner[a]Milling machine	96,376	1	96,376	23.04	**<0.001**	Scanner[a]Milling machine	22,253	1	22,253	1.92	0.166
Scanner[a]Material	29,665	1	29,665	7.09	**0.008**	Scanner[a]Material	10,613	1	10,613	0.92	0.338
Milling machine[a]Material	83,596	1	83,596	19.98	**<0.001**	Milling machine[a]Material	1798	1	1798	0.16	0.693
Scanner[a]Milling machine[a]Material	1	1	1	0.00	0.986	Scanner[a]Milling machine[a]Material	135,946	1	135,946	11.75	**0.001**
Pulpal Space						*Fatigue Failure Load*					
Factors	SS	DF	MS	F	*P*	Factors	SS	DF	MS	F	*P*
Scanner device	7316	1	7316	0.92	0.338	Scanner device	153,125	1	153,125	3.12	0.081
Milling machine	544,188	1	544,188	68.28	**<0.001**	Milling machine	125	1	125	0.00	0.959
Material	180	1	180	0.02	0.881	Material	3.31	1	3.31	675.64	**<0.001**
Scanner[a]Milling machine	6675	1	6675	0.84	0.361	Scanner[a]Milling machine	351,125	1	351,125	7.16	**0.009**
Scanner[a]Material	13,760	1	13,760	1.73	0.189	Scanner[a]Material	21,125	1	21,125	0.43	0.514
Milling machine[a]Material	16,544	1	16,544	2.08	0.150	Milling machine[a]Material	210,125	1	210,125	4.28	**0.042**
Scanner[a]Milling machine[a]Material	19,482	1	19,482	2.44	0.119	Scanner[a]Milling machine[a]Material	120,125	1	120,125	2.45	0.122

SS, Sum of squares; DF, degrees of freedom; MS, Mean square.
[a] Significant p-values (<.05) are marked in bold letters.

Table 2
Mean and standard deviation (in μm) for the pairwise comparisons for marginal and internal adaptation data considering the factors IOS, milling machine, and restorative material isolated.

Factor		Marginal gap	Cervical-axial angle	Axio-occlusal angle	Pulpal angle	Pulpal space
Scanner	**TR**	120.3 (91.0)^{B}	185.3 (68.7)^{B}	132.6 (62.0)^{A}	225.5 (114.9)^{A}	230.9 (74.3)^{A}
	PS	106.9 (82.1)^{A}	175.8 (63.4)^{A}	142.8 (68.7)^{B}	218.9 (107.7)^{A}	238.7 (112.9)^{A}
Milling machine	**CR**	107.1 (66.3)^{A}	172.4 (56.8)^{A}	135.9 (61.9)^{A}	204.7 (118.7)^{A}	235.4 (96.1)^{A}
	PM	120.1 (103.1)^{B}	188.6 (73.6)^{B}	139.5 (69.1)^{A}	239.6 (99.5)^{B}	234.2 (82.3)^{A}
Restorative material	**LD**	119.3 (74.4)^{B}	177.3 (53.3)^{A}	138.9 (63.8)^{A}	242.8 (99.6)^{B}	268.5 (106.3)^{B}
	RC	107.9 (97.5)^{A}	183.7 (76.9)^{A}	136.5 (67.5)^{A}	201.6 (119.6)^{A}	201.1 (83.5)^{A}

[a]Different capital letters according to 3-way ANOVA with Tukey's post hoc for each measuring point separately (α = .05).

wavy pattern from the diamond burs is noticeable in RC endocrowns (Fig. 6). This pattern is less pronounced in LD endocrowns, but a cracked margin is visible in this material regardless of the milling machine used (Fig. 6). It is also noteworthy that the burs promoted different topography patterns depending on the restoration region milled. As they approached the axial walls and marginal areas, the pattern became more linear, which can be attributed to the burs' lateral contact during milling. Meanwhile, in the occlusal and pulpal walls, the marks corresponded to the burs' tip (Fig. 6).

4. Discussion

This study showed that all studied factors; scanner device, milling machine, restorative materials, and digital workflows, had a significant influence on the marginal/internal fit and fatigue behavior of CAD-CAM milled endocrowns. Therefore, all four tested hypotheses were accepted.

Achieving a proper fit is crucial to the success and predictability of clinical rehabilitation, especially when considering the endocrowns limited preparation height (Bindl et al., 2006; Dartora et al., 2019). Therefore, the workflow used to fabricate these elements has an important role in ensuring properly adapted restorations (Ayres et al., 2023). However, the complexity of the endocrown preparation, particularly the depth of the pulpal chamber, represents a challenge, especially concerning digital image acquisition with intraoral scanners and the reproducibility of details by the milling machine (Ayres et al., 2023; Baldi et al., 2023; Gurpinar and Tak, 2022). This challenge was corroborated herein (Tables 2 and 3) as the misfit at the pulpal angle and space generally exceeded the planned space of 120 μm, indicating over milling (Zheng et al., 2022b; Zimmermann et al., 2019).

As mentioned before, IOS relies on light-dependent technology, where the length and depth of the acquisition field critically affect restoration fit (Baldi et al., 2023; Gurpinar and Tak, 2022). Previous studies have shown that the Primescan exhibits higher trueness compared to the TRIOS 3, particularly for complex restoration designs (Gurpinar and Tak, 2022). This difference can be attributed to variations in acquisition principles and the depth of field. Primescan uses a combination of technologies, including active triangulation and dynamic confocal microscopy, while the TRIOS 3 relies only on a simplified version of confocal microscopy, which captures in-focus images at selected depths (Gaintantzopoulou and El-Damanhoury, 2016; Logozzo

Table 3
Results for marginal and internal fit (μm), depicting means, standard deviations (SD), and 95% confidence intervals (95% CI) for each group obtained through 3-way ANOVA and Tukey's post-hoc for the triple factor association (Scanner[a]Milling machine[a]Material).

Groups	Marginal gap (n = 120)		Cervical-axial angle (n = 120)		Axial-occlusal angle (n = 240)		Pulpal Angle (n = 120)		Pulpal Space (n = 60)	
	Mean (SD)	CI 95%	Mean (SD)	CI 95%	Mean (SD)	CI 95%	Mean (SD)	CI 95%	Mean (SD)	CI 95%
TR-CR-LD	144.5 (80.2) ^{D}	130.0–159.0	184.1 (65.2) ^{ABC}	172.3–195.9	149.6 (55.8) ^{BC}	142.5–156.7	210.0 (75.3) ^{BC}	196.4–223.6	266.3 (42.7) ^{CD}	255.3–277.3
TR-CR-RC	109.1 (75.2) ^{ABC}	95.5–122.7	162.9 (63.6) ^{A}	151.5–174.4	126.1 (56.2) ^{A}	119.0–133.3	272.6 (163.0) ^{D}	243.1–302.1	255.4 (64.4) ^{BCD}	238.7–272.0
TR-PM-LD	119.4 (97.8) ^{BCD}	101.7–137.0	188.6 (57.3) ^{BC}	178.2–198.9	125.9 (64.9) ^{A}	117.6–134.1	199.4 (85.9) ^{AB}	183.9–215.0	207.4 (74.6) ^{AB}	188.2–226.7
TR-PM-RC	108.3 (104.0) ^{ABC}	89.5–127.1	205.5 (80.6) ^{C}	191.0–220.1	128.7 (67.4) ^{A}	120.1–137.3	219.9 (101.7) ^{BC}	201.5–238.3	194.5 (83.9) ^{A}	172.8–216.1
PS-CR-LD	96.3 (41.2) ^{AB}	88.9–103.8	167.8 (42.3) ^{AB}	160.2–175.4	137.9 (77.1) ^{AB}	128.1–147.7	243.5 (135.5) ^{CD}	219.0–267.9	283.6 (172.8) ^{D}	283.6–328.3
PS-CR-RC	78.6 (39.2) ^{A}	71.5–85.6	174.9 (51.5) ^{AB}	165.6–184.2	130.0 (53.5) ^{A}	123.2–136.8	245.2 (64.2) ^{CD}	233.6–256.8	268.5 (33.7) ^{D}	259.9–277.3
PS-PM-LD	117.2 (58.5) ^{BCD}	106.7–127.8	168.8 (42.4) ^{AB}	161.2–176.5	142.4 (52.4) ^{AB}	135.7–149.1	166.1 (73.8) ^{A}	152.7–179.4	184.3 (42.0) ^{A}	173.5–195.2
PS-PM-RC	135.6 (136.4) ^{CD}	110.9–160.2	191.6 (97.7) ^{BC}	174.0–209.3	161.0 (83.0) ^{C}	150.5–171.6	220.9 (121.2) ^{BC}	199.0–242.8	218.3 (111.5) ^{ABC}	189.5–247.1

TR, TRIOS 3; PS, Primescan; CR, CEREC MC XL; PM, PrograMill PM7; LD, lithium disilicate; RC, resin composite.
[a] Different capital letters in each column indicate statistical differences according to 3-way ANOVA and Tukey's post-hoc for the triple factor association (Scanner*Milling machine*Material) with α= .05.

Table 4
Mean, standard deviation, and confidence interval (CI 95%) of fatigue failure load (FFL) and number of cycles for failure (CFF) of the different tested groups. Weibull Modulus (*m*) for FFL is also expressed.

Groups	FFL			CFF	
	Mean (SD)[a]	CI 95%	*m*[b]	Mean (SD)[a]	CI 95%
TR-CR-LD	835 (97) ^{D}	765–905	8.5 (5.1–12.5) ^{A}	152,000 (19,465) ^{D}	138,075–165,924
TR-CR-RC	2270 (279) ^{A}	2070–2470	10.7 (6.1–16.9) ^{A}	362,000 (27,908) ^{A}	342,035–381,965
TR-PM-LD	885 (85) ^{CD}	824–946	12.3 (7.1–19.1) ^{A}	163,000 (18,135) ^{CD}	150,027–175,973
TR-PM-RC	1960 (217) ^{B}	1805–2115	11.1 (6.5–17.0) ^{A}	331,000 (24,472) ^{B}	313,494–348,506
PS-CR-LD	835 (108) ^{D}	758–912	8.1 (4.8–12.2) ^{A}	152,000 (21,628) ^{D}	136,528–167,472
PS-CR-RC	2180 (326) ^{AB}	1947–2413	7.6 (4.4–11.8) ^{A}	354,000 (32,472) ^{AB}	330,771–377,229
PS-PM-LD	995 (159) ^{C}	881–1109	6.8 (4.0–10.4) ^{A}	184,000 (31,780) ^{C}	161,266–206,734
PS-PM-RC	2290 (328) ^{A}	2055–2525	7.6 (4.5–11.7) ^{A}	364,000 (32,812) ^{A}	340,528–284,473

TR, TRIOS 3; PS, Primescan; CR, CEREC MC XL; PM, PrograMill PM7; LD, lithium disilicate; RC, resin composite.
[a] Different capital letters in each column indicate statistical differences according to Kaplan-Meier and log-rank (Mantel-Cox) with α= .05.
[b] Similar capital letters indicate statistical similarities due to confidence interval overlapping between groups.

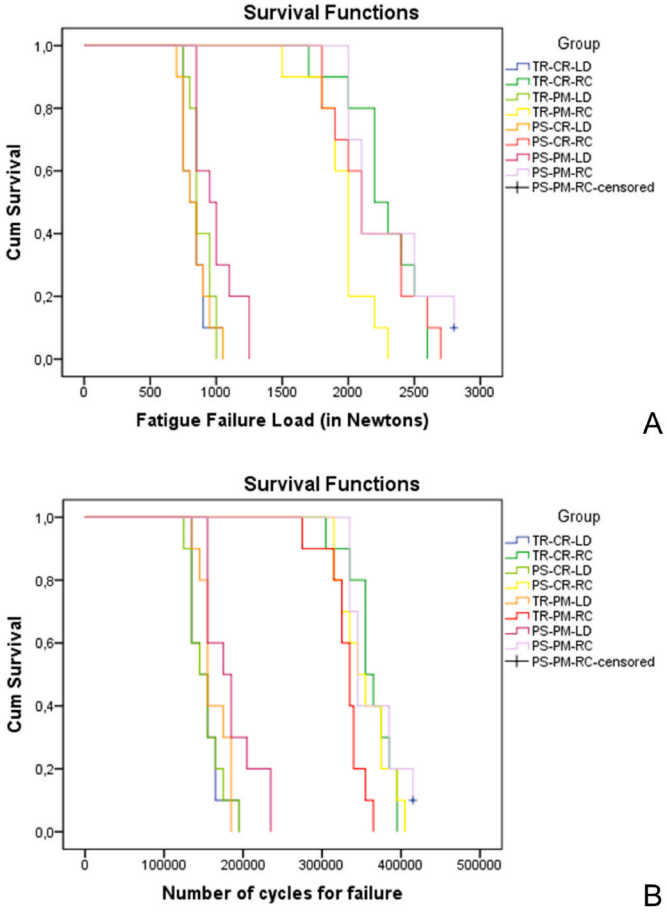

Fig. 4. Survival plots for the tested groups considering the fatigue failure load (A) and number of cycles for failure (B) data. Censored data represents specimens that survived the fatigue testing protocol.

et al., 2014). This, coupled with the shallower depth of field for the TRIOS 3 (14 mm) (Zhang et al., 2021) compared to the Primescan (20 mm), may explain the fit differences at various points. The Primescan resulted in better marginal and cervical-axial angle fit, whereas the TRIOS 3 outperformed the axio-occlusal angle, which is an easier point to be scanned. Nonetheless, both IOS struggled to consistently capture the pulpal chamber preparation, as this region is inherently more difficult to be scanned (Gaintantzopoulou and El-Damanhoury, 2016; Ghoul et al., 2020; Gurpinar and Tak, 2022).

Apart from the number of axes (4 vs. 5), the milling machines also differ in the diamond burs used during the subtractive process. These

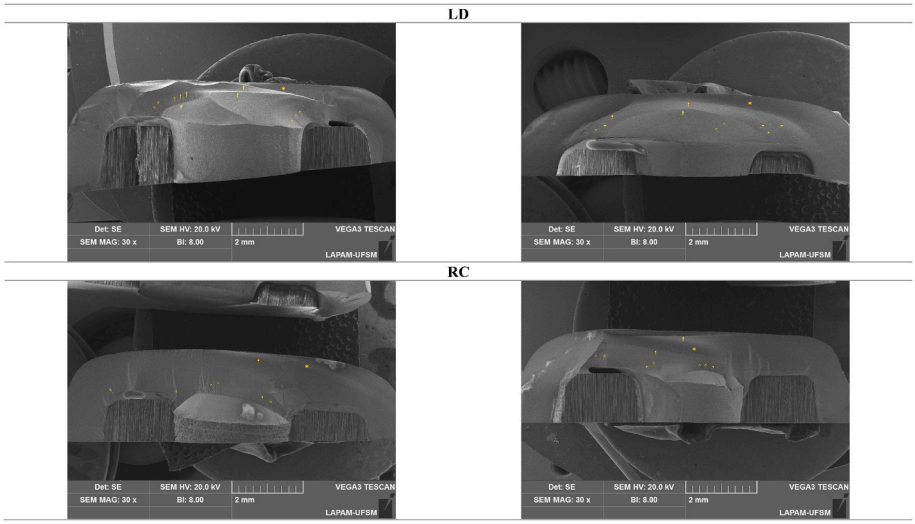

Fig. 5. Representative fractographic analysis of the different materials – lithium disilicate and resin composite under SEM. Dashed arrows indicate the direction of crack propagation, the straight arrows indicate the arrest lines, and the asterisk indicates the compression curl. It is possible to visualize that the failure started from the restoration inner surface and continued forward to the occlusal surface.

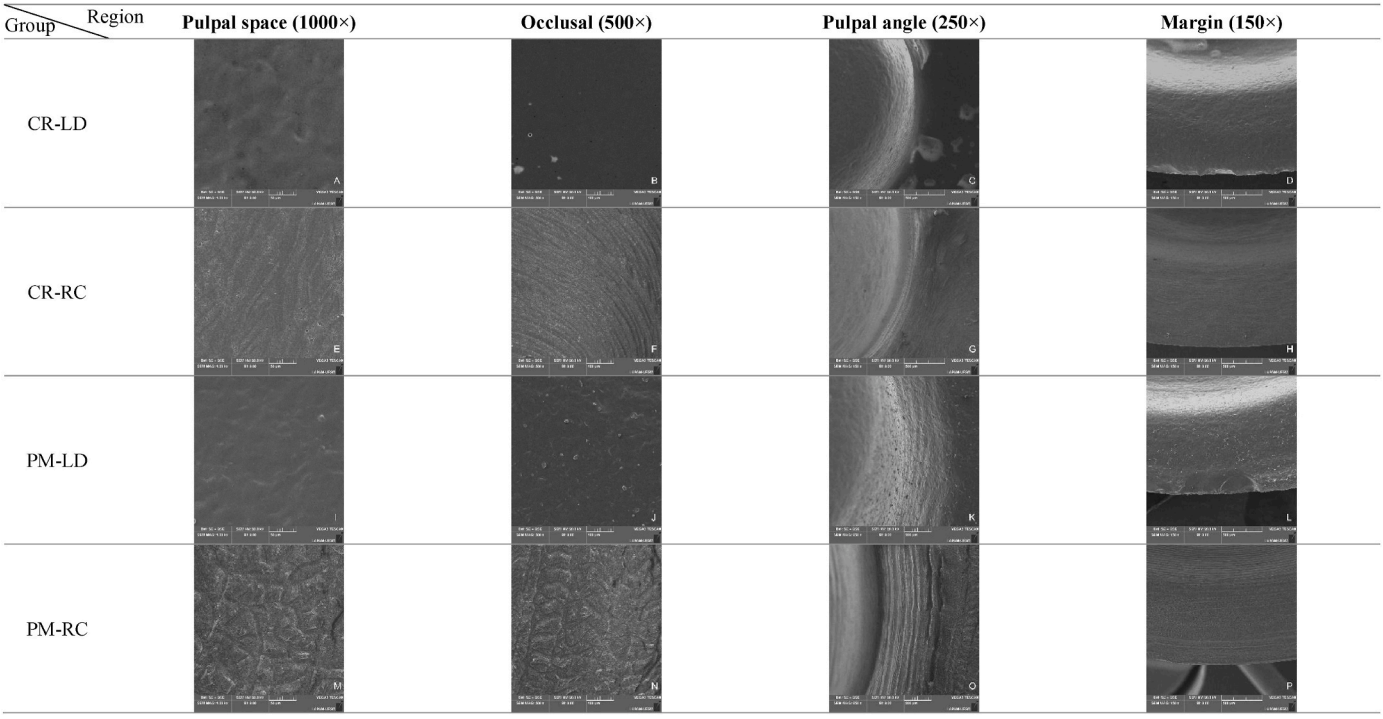

Fig. 6. Surface pattern resultant from the milling machines and the 2 materials. In the RC endocrowns, a wavy pattern is visible resulting from milling in the PM7, which is not noticeable in the LD endocrowns. Despite that, at the margins, the LD restorations showed chipping.

differences include the number of burs (2 vs. 3), the diameter size (1.35 + 1.75 mm vs. 2.8 + 2.0 + 1.0 mm), rotation speed (42,000 vs. 60,000 rpm), and the milling path (Alghazzawi, 2016). In this study, the CEREC MC XL milling machine (4-axis) demonstrated better marginal and cervical-axial angle fit, while the PrograMill PM7 (5-axis) resulted in better pulpal angle and pulpal space fit. This may be explained by the different milling paths (Bosch et al., 2014), which are evident in the topographic analysis using SEM. The 4-axis machine appears to yield a more uniform and smoother pattern in the margin and cervical angle, while the 5-axis, which employs a smaller tip-bur for a detailed inner surface process, resulted in a considerably smaller gap in the pulp chamber area (Ayres et al., 2023; El Ghoul and Salameh, 2021; Zimmermann et al., 2019).

The choice of restorative material in the final stage of the digital workflow significantly affects the marginal and internal fit (Papadiochou and Pissiotis, 2018). Previous studies have indicated that differences in fit were expected considering the contrasting microstructures and machinability between glass-ceramic and resin composite materials (Ayres et al., 2023; Ghoul et al., 2020; Rippe et al., 2017; Zheng et al., 2022b; Zimmermann et al., 2019). The brittle nature of lithium disilicate ceramic and its susceptibility to chipping during the milling process, especially at the margin (Curran et al., 2017; Rippe et al., 2017; Zimmermann et al., 2019), led to increased misfit in this area compared to the resin composite material, mainly when using the TR-CR workflow.

This is visibly demonstrated in the SEM topographic figures (Fig. 6). However, no difference was observed between the restorative materials in the cervical-axial angle, axio-occlusal angle, and pulpal space. It is known that angle areas and pulpal chamber space are inherently more challenging to accurately reproduce through milling, which seems to be the primary factor (Zheng et al., 2022b; Zimmermann et al., 2019). Nonetheless, in the pulpal angle area, the lithium disilicate restorations exhibited a better fit compared to the resin composite ones, particularly for the TR-CR and PS-PM workflows (Ghoul et al., 2020; Hassouneh et al., 2023). Despite the advantages of resin composite material in terms of machinability during the subtractive process, it may also result in material over-removal in some regions due to its softer nature compared to LD (Coldea et al., 2015).

Despite the interaction between scanners, milling machines, and restorative material not significantly affecting the fatigue failure load of endocrowns according to the factorial analysis, the factors material, paired association between scanner*milling machine, and between milling machine*material were statistically significant (Table 1). Thus, some noteworthy features can be highlighted. Resin composite exhibited higher survival rates compared to lithium disilicate ceramic irrespective of the scanner and milling device used (Pivetta Rippe et al., 2019). This can be attributed to the lower elastic modulus of resin-based materials compared to ceramics, along with their resilient properties, favoring their mechanical behavior, especially when adhesively bonded (Al-Dabbagh, 2021; Dartora et al., 2019; Zheng et al., 2021, 2022a). Among the resin composite restorations, slight statistical differences in fatigue data were found when comparing TR-PM-RC to TR-CR-RC and PS-PM-RC. However, these differences may not be great enough to induce clinically relevant effects. Additionally, it is worth mentioning that one specimen in the PS-PM-RC group survived the fatigue test (Fig. 4). Similarly, statistical differences were found among lithium disilicate groups (PS-PM-LD compared to PS-CR-LD and TR-CR-LD), but considering the overlapping of confidence intervals, these differences may also not be clinically relevant. Therefore, the fatigue behavior of the endocrowns fabricated with different workflows seems to be highly dependent on the restorative material microstructure (Ayres et al., 2023; Pivetta Rippe et al., 2019; Sedrez-Porto et al., 2019, 2020).

It is important to highlight that the failures initiated from the axio-occlusal angle, known as a stress concentration area (Tribst et al., 2018, 2021; Zheng et al., 2021). Thus, it is logical to assume that the discrepancies noted at the pulpal preparation, related to the depth of the pulpal chamber, are not in a critical area. Based on that, it is also logical to understand why the failures herein were more related to differences in material properties rather than variations in the digital workflow. It is also important to highlight that it was considered an endocrown with ferrule preparation herein; however, recent studies have shown that this does not improve the marginal adaptation and the mechanical behavior of endocrowns restoration (Mannocci et al., 2022; Rocca et al., 2021). Therefore, for future studies considering endocrowns restoration fit and fatigue behavior, the ferrule preparation can be omitted. Finally, it is important to emphasize that this study has some inherent limitations, as it did not consider an anatomical restoration, and it did not include an assessment of aging effects. Nevertheless, the authors are not aware of any previous study that has evaluated endocrowns made with different digital workflows and restorative materials and their impact on fatigue behavior associated with marginal/internal fit.

5. Conclusion

The TRIOS 3 yielded in better axio-occlusal fit, the Primescan exhibited a better fit for marginal gap and cervical-axial angle. However, the choice of IOS did not affect the pulpal chamber preparation fit. CEREC MC XL resulted in better marginal and cervical-axial fit, while the PrograMill PM7 presented better pulpal chamber fit. The mechanical fatigue behavior of the endocrowns was not affected by the choice of the scanner or the milling machines, however, the restorative material played a significant role. The resin-based restorations resulted in a higher survival rate and smoother margins with better marginal fit compared to the lithium disilicate ones.

Support/sponsorship

This work is part of the fulfillment of the requirements of the Ph.D. degree (R.O.P.) in the Post-Graduate Program in Oral Sciences at the Faculty of Dentistry, Universidade Federal de Santa Maria (Rio Grande do Sul State, Brazil). Besides, this study was partially financed by the Brazilian National Council for Scientific and Technological Development – CNPq (R.O.P. doctorate scholarship, project #140118/2022-5; R.V.M. Postdoctoral Scholarship; Project no. 151004/2022-6; G.K.R.P. research productivity scholarship Pq2, process number #304665/2022-3), by the Brazilian Federal Agency for Coordination of Improvement of Higher Education Personnel – CAPES (Finance code 001, L.S.R. Doctorate's scholarship), and by the Foundation to Research Support of the Rio Grande do Sul State – FAPERGS (project #21/2551-0001961-1).

CRediT authorship contribution statement

Rafaela Oliveira Pilecco: Writing – original draft, Visualization, Methodology, Investigation, Formal analysis, Data curation, Conceptualization. **Lucas Saldanha da Rosa:** Writing – review & editing, Methodology, Investigation, Formal analysis. **Andrea Baldi:** Writing – review & editing, Software, Methodology, Investigation, Formal analysis. **Renan Vaz Machry:** Writing – review & editing, Methodology, Investigation, Formal analysis. **João Paulo Mendes Tribst:** Writing – review & editing, Methodology, Investigation. **Luiz Felipe Valandro:** Writing – review & editing, Methodology, Investigation, Funding acquisition, Conceptualization. **Cornelis Johannes Kleverlaan:** Writing – review & editing, Methodology, Investigation. **Nicola Scotti:** Writing – review & editing, Supervision, Software, Methodology, Investigation, Conceptualization. **Gabriel Kalil Rocha Pereira:** Writing – review & editing, Supervision, Project administration, Methodology, Investigation, Funding acquisition, Conceptualization.

Declaration of competing interest

The authors declare that they have no known competing financial interests or personal relationships that could have appeared to influence the work reported in this paper.

Data availability

Data will be made available on request.

Acknowledgments

We especially thank Ivoclar AG for donating some of the used materials. We emphasize that the supporting institutions did not have any role in the study design, data collection or analysis, the decision to publish, or in preparing the manuscript.

References

Abduljawad, D.E., Rayyan, M.R., 2022. Marginal and internal fit of lithium disilicate endocrowns fabricated using conventional, digital, and combination techniques. J. Esthetic Restor. Dent. 34, 707–714. https://doi.org/10.1111/jerd.12902.

Alajaji, N.K., Bardwell, D., Finkelman, M., Ali, A., 2017. Micro-CT evaluation of ceramic inlays: comparison of the marginal and internal fit of five and three Axis CAM systems with a heat press technique. J. Esthetic Restor. Dent. 29, 49–58. https://doi.org/10.1111/jerd.12271.

Al-Dabbagh, R.A., 2021. Survival and success of endocrowns: a systematic review and meta-analysis. J. Prosthet. Dent 125, 415.e1–415.e9. https://doi.org/10.1016/j.prosdent.2020.01.011.

Alghazzawi, T.F., 2016. Advancements in CAD/CAM technology: options for practical implementation. J Prosthodont Res. https://doi.org/10.1016/j.jpor.2016.01.003.

Ayres, G., Parize, H., Mendonça, L.M., Kubata, B.R., Tirapelli, C., 2023. Is the digital workflow more efficient for manufacturing partial-coverage restorations? A systematic review. J. Prosthet. Dent. https://doi.org/10.1016/j.prosdent.2023.08.005.

Baldi, A., Comba, A., Rozzi, D., Rocha Pereira, G.K., Valandro, L.F., Michelotto Tempesta, R., Scotti, N., 2023. Does partial adhesive preparation design and finish line depth influence trueness and precision of intraoral scanners? J. Prosthet. Dent. https://doi.org/10.1016/j.prosdent.2023.01.017.

Bindl, A., Richter, B., Mörmann, W.H., 2006. Survival of ceramic computer-aided design/manufacturing crowns bonded to preparations with reduced macroretention geometry. J. Prosthet. Dent 95, 81. https://doi.org/10.1016/j.prosdent.2005.09.002.

Blatz, M.B., Conejo, J., 2019. The current state of chairside digital dentistry and materials. Dent. Clin. 63, 175–197. https://doi.org/10.1016/j.cden.2018.11.002.

Bosch, G., Ender, A., Mehl, A., 2014. A 3-dimensional accuracy analysis of chairside CAD/CAM milling processes. J. Prosthet. Dent 112, 1425–1431. https://doi.org/10.1016/j.prosdent.2014.05.012.

Coldea, A., Fischer, J., Swain, M.V., Thiel, N., 2015. Damage tolerance of indirect restorative materials (including PICN) after simulated bur adjustments. Dent. Mater. 31, 684–694. https://doi.org/10.1016/j.dental.2015.03.007.

Curran, P., Cattani-Lorente, M., Wiskott, H.W.A., Durual, S., Scherrer, S.S., 2017. Grinding damage assessment for CAD-CAM restorative materials. Dent. Mater. 33, 294–308. https://doi.org/10.1016/j.dental.2016.12.004.

Da Fonseca, G.F., De Andrade, G.S., Dal Piva, A.M.D.O., Tribst, J.P.M., Borges, A.L.S., 2018. Computer-aided design finite element modeling of different approaches to rehabilitate endodontically treated teeth. J. Indian Prosthodont. Soc. 18 (4), 329–335. https://doi.org/10.4103/jips.jips_168_18.

Dalla-Nora, F., Da Rosa, L.S., Pereira, G.K.R., Valandro, L.F., Rippe, M.P., 2024. Is dentin analogue material a viable substitute for human dentin in fatigue behavior studies? J. Mech. Behav. Biomed. Mater. 150, 106312 https://doi.org/10.1016/j.jmbbm.2023.106312.

Dartora, G., Rocha Pereira, G.K., Varella de Carvalho, R., Zucuni, C.P., Valandro, L.F., Cesar, P.F., Caldas, R.A., Bacchi, A., 2019. Comparison of endocrowns made of lithium disilicate glass-ceramic or polymer-infiltrated ceramic networks and direct composite resin restorations: fatigue performance and stress distribution. J. Mech. Behav. Biomed. Mater. 100, 103401 https://doi.org/10.1016/j.jmbbm.2019.103401.

Dartora, N.R., de Conto Ferreira, M.B., Moris, I.C.M., Brazão, E.H., Spazin, A.O., Sousa-Neto, M.D., Silva-Sousa, Y.T., Gomes, E.A., 2018. Effect of intracoronal depth of teeth restored with endocrowns on fracture resistance: in vitro and 3-dimensional finite element analysis. J. Endod. 44, 1179–1185. https://doi.org/10.1016/j.joen.2018.04.008.

Duan, Y., Griggs, J.A., 2015. Effect of elasticity on stress distribution in CAD/CAM dental crowns: glass ceramic vs. polymer-matrix composite. J. Dent. 43, 742–749. https://doi.org/10.1016/j.jdent.2015.01.008.

El Ghoul, W., Salameh, Z., 2021. Marginal and internal adaptation of lithium disilicate endocrowns fabricated by heat-pressable and subtractive techniques. J. Prosthodont. 30, 509–514. https://doi.org/10.1111/jopr.13272.

Fages, M., Bennasar, B., 2013. The endocrown: a different type of all-ceramic reconstruction for molars. J. Can. Dent. Assoc. 79 d140–d140.

Freitas, B.N. De, Tonin, B.S.H.H., Macedo, A.P., Santos, T.M.P., d, G.C.G.C., De Mattos, M., Hotta, T.H., Matsumoto, W., dos Santos, T.M.P., d, G.C.G.C., De Mattos, M., Hotta, T.H., Matsumoto, W., 2020. Adaptation accuracy of milled lithium disilicate crowns: a 2D and 3D microCT analysis. J. Esthetic Restor. Dent. 32, 403–409. https://doi.org/10.1111/jerd.12574.

Gaintantzopoulou, M., El-Damanhoury, H., 2016. Effect of preparation depth on the marginal and internal adaptation of computer-aided design/computer-assisted manufacture endocrowns. Operat. Dent. 41, 607–616. https://doi.org/10.2341/15-146-L.

Ghoul, W.A. El, Özcan, M., Ounsi, H., Tohme, H., Salameh, Z., 2020. Effect of different CAD-CAM materials on the marginal and internal adaptation of endocrown restorations: an in vitro study. J. Prosthet. Dent 123, 128–134. https://doi.org/10.1016/J.PROSDENT.2018.10.024.

Govare, N., Contrepois, M., 2020. Endocrowns: a systematic review. J. Prosthet. Dent 123, 411–418.e9. https://doi.org/10.1016/j.prosdent.2019.04.009.

Gurpinar, B., Tak, O., 2022. Effect of pulp chamber depth on the accuracy of endocrown scans made with different intraoral scanners versus an industrial scanner: an in vitro study. J. Prosthet. Dent 127, 430–437. https://doi.org/10.1016/j.prosdent.2020.08.034.

Hassouneh, L., Jum'ah, A., Ferrari, M., Wood, D.J., 2023. A micro-computed tomography analysis of marginal and internal fit of endocrowns fabricated from three CAD/CAM materials. Operat. Dent. 48, 79–89. https://doi.org/10.2341/21-105-L.

He, J., Zheng, Z., Wu, M., Zheng, C., Zeng, Y., Yan, W., 2021. Influence of restorative material and cement on the stress distribution of endocrowns: 3D finite element analysis. BMC Oral Health 21. https://doi.org/10.1186/s12903-021-01865-w.

Holmes, J.R., Bayne, S.C., Holland, G.A., Sulik, W.D., 1989. Considerations in measurement of marginal fit. J. Prosthet. Dent 62, 405–408. https://doi.org/10.1016/0022-3913(89)90170-4.

Kelly, J.R., Rungruanganunt, P., Hunter, B., Vailati, F., 2010. Development of a clinically validated bulk failure test for ceramic crowns. J. Prosthet. Dent 104, 228–238. https://doi.org/10.1016/S0022-3913(10)60129-1.

Kruzic, J.J., Arsecularatne, J.A., Tanaka, C.B., Hoffman, M.J., Cesar, P.F., 2018. Recent advances in understanding the fatigue and wear behavior of dental composites and ceramics. J. Mech. Behav. Biomed. Mater. https://doi.org/10.1016/j.jmbbm.2018.08.008.

Lenz, U., Bacchi, A., Della Bona, A., 2023. Biomechanical performance of endocrown and core-crown restorations: a systematic review. J. Esthetic Restor. Dent. https://doi.org/10.1111/jerd.13119.

Logozzo, S., Zanetti, E.M., Franceschini, G., Kilpelä, A., Mäkynen, A., 2014. Recent advances in dental optics – Part I: 3D intraoral scanners for restorative dentistry. Opt Laser. Eng. 54, 203–221. https://doi.org/10.1016/j.optlaseng.2013.07.017.

Mannocci, F., Bitter, K., Sauro, S., Ferrari, P., Austin, R., Bhuva, B., 2022. Present status and future directions: the restoration of root filled teeth. Int. Endod. J. https://doi.org/10.1111/iej.13796.

Martini, A.P., de Souza, F.I., Anchieta, R.B., de Almeida, E.O., Junior, A.C.F., Rocha, E.P., 2019. Influence of resin cement thickness and temperature variation on mechanical behavior of dental ceramic fragment restoration. Comput. Methods Biomech. Biomed. Eng. 22, 409–417. https://doi.org/10.1080/10255842.2018.1560428.

May, L.G., Kelly, J.R., Bottino, M.A., Hill, T., 2012. Effects of cement thickness and bonding on the failure loads of CAD/CAM ceramic crowns: multi-physics FEA modeling and monotonic testing. Dent. Mater. 28 https://doi.org/10.1016/j.dental.2012.04.033.

Missau, T., Venturini, A.B., Pereira, G.K.R., Prochnow, C., Valandro, L.F., Rippe, M.P., 2018. Fatigue failure load of restored premolars: effect of etching the intaglio surface of ceramic inlays with hydrofluoric acid at different concentrations. Operat. Dent. 43, E81–E91. https://doi.org/10.2341/16-345-L.

Nawafleh, N.A., Mack, F., Evans, J., Mackay, J., Hatamleh, M.M., 2013. Accuracy and reliability of methods to measure marginal adaptation of crowns and FDPs: a literature review. J. Prosthodont. 22, 419–428. https://doi.org/10.1111/jopr.12006.

Papadiochou, S., Pissiotis, A.L., 2018. Marginal adaptation and CAD-CAM technology: a systematic review of restorative material and fabrication techniques. J. Prosthet. Dent 119, 545–551. https://doi.org/10.1016/j.prosdent.2017.07.001.

Pilecco, R.O., Dapieve, K.S., Baldi, A., Valandro, L.F., Scotti, N., Pereira, G.K.R., 2023. Comparing the accuracy of distinct scanning systems and their impact on marginal/internal adaptation of tooth-supported indirect restorations. A scoping review. J. Mech. Behav. Biomed. Mater. 144, 105975 https://doi.org/10.1016/j.jmbbm.2023.105975.

Pilecco, R.O., Machry, R.V., Baldi, A., Tribst, J.P.M., Sarkis-Onofre, R., Valandro, L.F., Kleverlaan, C.J., Scotti, N., Pereira, G.K.R., 2024. Influence of CAD-CAM milling strategies on the outcome of indirect restorations: a scoping review. J. Prosthet. Dent. https://doi.org/10.1016/j.prosdent.2024.02.021.

Pivetta Rippe, M., Monaco, C., Missau, T., Wandscher, V.F., Volpe, L., Scotti, R., Bottino, M.A., Valandro, L.F., 2019. Survival rate and load to failure of premolars restored with inlays: an evaluation of different inlay fabrication methods. J. Prosthet. Dent 121, 292–297. https://doi.org/10.1016/j.prosdent.2018.03.019.

Rippe, M.P., Monaco, C., Volpe, L., Bottino, M.A., Scotti, R., Valandro, L.F., 2017. Different methods for inlay production: effect on internal and marginal adaptation, adjustment time, and contact point. Operat. Dent. 42, 436–444. https://doi.org/10.2341/16-093-L.

Rocca, G., Canneto, J., Scotti, N., Daher, R., Feilzer, A., Saratti, C., Krejci, I., 2021. Restoration of severely damaged endodontically treated premolars: influence of the ferrule effect on marginal integrity and fracture load of resin nano-ceramic CAD-CAM endocrowns. Operat. Dent. 46, 650–660. https://doi.org/10.2341/20-081-L.

Saratti, C.M., Rocca, G.T., Durual, S., Lohbauer, U., Ferracane, J.L., Scherrer, S.S., 2021. Fractography of clinical failures of indirect resin composite endocrown and overlay restorations. Dent. Mater. 37, e341–e359. https://doi.org/10.1016/j.dental.2021.02.002.

Schestatsky, R., Zucuni, C.P., Venturini, A.B., de Lima Burgo, T.A., Bacchi, A., Valandro, L.F., Pereira, G.K.R., 2019. CAD-CAM milled versus pressed lithium-disilicate monolithic crowns adhesively cemented after distinct surface treatments: fatigue performance and ceramic surface characteristics. J. Mech. Behav. Biomed. Mater. 94, 144–154. https://doi.org/10.1016/j.jmbbm.2019.03.005.

Sedrez-Porto, J.A., Münchow, E.A., Cenci, M.S., Pereira-Cenci, T., 2020. Which materials would account for a better mechanical behavior for direct endocrown restorations? J. Mech. Behav. Biomed. Mater. 103 https://doi.org/10.1016/j.jmbbm.2019.103592.

Sedrez-Porto, J.A., Münchow, E.A., Valente, L.L., Cenci, M.S., Pereira-Cenci, T., 2019. New material perspective for endocrown restorations: effects on mechanical performance and fracture behavior. Braz. Oral Res. 33 https://doi.org/10.1590/1807-3107bor-2019.vol33.0012.

Seo, D., Yi, Y., Roh, B., 2009. The effect of preparation designs on the marginal and internal gaps in Cerec3 partial ceramic crowns. J. Dent. 37, 374–382. https://doi.org/10.1016/j.jdent.2009.01.008.

Soliman, M., Alzahrani, G., Alabdualataif, F., Eldwakhly, E., Alsamady, S., Aldegheishem, A., Abdelhafeez, M.M., 2022. Impact of ceramic material and preparation design on marginal fit of endocrown restorations. Materials 15. https://doi.org/10.3390/ma15165592.

Tribst, J.P.M., Dal Piva, A.M. de O., Jager, N., Bottino, M.A., Kok, P., Kleverlaan, C.J., 2021. Full-crown versus endocrown approach: a 3D-analysis of both restorations and the effect of ferrule and restoration material. J. Prosthodont. 30, 335–344. https://doi.org/10.1111/jopr.13244.

Tribst, J.P.M., Dal Piva, A.M. de O., Madruga, C.F.L., Valera, M.C., Borges, A.L.S., Bresciani, E., de Melo, R.M., 2018. Endocrown restorations: influence of dental remnant and restorative material on stress distribution. Dent. Mater. 34, 1466–1473. https://doi.org/10.1016/j.dental.2018.06.012.

Vág, J., Nagy, Z., Bocklet, C., Kiss, T., Nagy, Á., Simon, B., Mikolicz, Á., Renne, W., 2020. Marginal and internal fit of full ceramic crowns milled using CADCAM systems on cadaver full arch scans. BMC Oral Health 20, 189. https://doi.org/10.1186/s12903-020-01181-9.

Valandro, L.F., Cadore-Rodrigues, A.C., Dapieve, K.S., Machry, R.V., Pereira, G.K.R., 2023. A brief review on fatigue test of ceramic and some related matters in Dentistry. J. Mech. Behav. Biomed. Mater. 138 https://doi.org/10.1016/J.JMBBM.2022.105607.

Velho, H.C., Dapieve, K.S., Pereira, G.K.R., Fraga, S., Valandro, L.F., Venturini, A.B., 2020. Accelerated loading frequency does not influence the fatigue behavior of polymer infiltrated ceramic network or lithium disilicate glass-ceramic restorations. J. Mech. Behav. Biomed. Mater. 110, 103905 https://doi.org/10.1016/j.jmbbm.2020.103905.

Venturini, A.B., Prochnow, C., May, L.G., Kleverlaan, C.J., Valandro, L.F., 2018. Fatigue failure load of feldspathic ceramic crowns after hydrofluoric acid etching at different concentrations. J. Prosthet. Dent 119, 278–285. https://doi.org/10.1016/j.prosdent.2017.03.021.

Vijayakumar, J.B., Varadan, P., Balaji, L., Rajan, M., Kalaiselvam, R., Saeralaathan, S., Ganesh, A., 2021. Fracture resistance of resin based and lithium disilicate endocrowns. Which is better? – a systematic review of in-vitro studies. Biomater Investig Dent 8, 104. https://doi.org/10.1080/26415275.2021.1932510.

Yildirim, G., Demir, C., Güven, M.Ç., Koç, O., Dalkiliç, E.E., 2022. Influence of fiber insertion and different material type on stress distribution in endocrown restorations: a 3D-FEA study. Comput. Methods Biomech. Biomed. Eng. 25, 1509–1519. https://doi.org/10.1080/10255842.2021.2019228.

Zhang, M., Hattori, M., Elbashti, M.E., Sumita, Y.I., 2021. Comparison of data acquisition for maxillectomy patients using two different intraoral scanners. Maxillofacial Prosthetics 44, 1–6.

Zhang, Y., Sailer, I., Lawn, B.R., 2013. Fatigue of dental ceramics. J. Dent. 41, 1135–1147. https://doi.org/10.1016/j.jdent.2013.10.007.

Zheng, Z., He, Y., Ruan, W., Ling, Z., Zheng, C., Gai, Y., Yan, W., 2021. Biomechanical behavior of endocrown restorations with different CAD-CAM materials: a 3D finite element and in vitro analysis. J. Prosthet. Dent 125, 890–899. https://doi.org/10.1016/J.PROSDENT.2020.03.009.

Zheng, Z., Sun, J., Jiang, L., Wu, Y., He, J., Ruan, W., Yan, W., 2022a. Influence of margin design and restorative material on the stress distribution of endocrowns: a 3D finite element analysis. BMC Oral Health 22. https://doi.org/10.1186/S12903-022-02063-Y.

Zheng, Z., Wang, H., Mo, J., Ling, Z., Zeng, Y., Zhang, Y., Wang, J., Yan, W., 2022b. Effect of virtual cement space and restorative materials on the adaptation of CAD-CAM endocrowns. BMC Oral Health 22, 580. https://doi.org/10.1186/s12903-022-02598-0.

Zimmermann, M., Valcanaia, A., Neiva, G., Mehl, A., Fasbinder, D., 2019. Three-Dimensional digital evaluation of the fit of endocrowns fabricated from different CAD/CAM materials. J. Prosthodont. 28 https://doi.org/10.1111/jopr.12770.